Exploring the regional pollution characteristics and meteorological formation mechanism of PM2.5 in North China þÿ d u r i n g 2 0 1 3 2 0 1 7

Li, Mingge

2020-01

Li , M , Wang , L , Liu , J , Gao , W , Song , T , Sun , Y , Li , L , Li , X , Wang , Y , Liu , L , Dällenbach , K , Paasonen , P J , Kerminen , V-M , Kulmala , M & Wang , Y 2020 , ' Exploring the regional pollution characteristics and meteorological formation mechanism of þÿ P M 2 . 5 i n N o r t h C h i n a d u r i n g 2 0 1 3 2 0 1 7 ' , E n v i r o n m e n t I n t e r n a t i o n a l ,

http://hdl.handle.net/10138/308974
https://doi.org/10.1016/j.envint.2019.105283

Environment International 134 (2020) 105283

Contents lists available at ScienceDirect

Environment International

journal homepage: www.elsevier.com/locate/envint

Exploring the regional pollution characteristics and meteorological formation mechanism of $PM_{2.5}$ in North China during 2013–2017

Mingge Li[a,g,1], Lili Wang[a,c,*,1], Jingda Liu[a,h], Wenkang Gao[a], Tao Song[a], Yang Sun[a], Liang Li[d], Xingru Li[f], Yonghong Wang[c], Lili Liu[e], Kaspar R. Daellenbach[c], Pauli J. Paasonen[c], Veli-Matti Kerminen[c], Markku Kulmala[c,i], Yuesi Wang[a,b,g,h]

[a] State Key Laboratory of Atmospheric Boundary Layer Physics and Atmospheric Chemistry (LAPC), Institute of Atmospheric Physics, Chinese Academy of Sciences, Beijing 100029, China
[b] Centre for Excellence in Atmospheric Urban Environment, Institute of Urban Environment, Chinese Academy of Science, Xiamen, Fujian 361021, China
[c] Institute for Atmospheric and Earth System Research / Physics, Faculty of Science, University of Helsinki, Finland
[d] China National Environmental Monitoring Center, Beijing 100012, China
[e] Tianjin Institute of Meteorological Science, Tianjin 300074, China
[f] Department of Chemistry, Analytical and Testing Center, Capital Normal University, Beijing 100048, China
[g] University of the Chinese Academy of Sciences, Beijing 100049, China
[h] Department of Atmospheric Physics, Nanjing University of Information Science & Technology, Nanjing 210044, China
[i] Aerosol and Haze Laboratory, Beijing Advanced Innovation Center for Soft Matter Science and Engineering, Beijing University of Chemical Technology, Beijing 100029, China

ARTICLE INFO

Keywords:
North China
$PM_{2.5}$
Regional pollution events
Identification of regional pollution type
Meteorological formation mechanism

ABSTRACT

In the last decade, North China (NC) has been one of the most populated and polluted regions in the world. The regional air pollution has had a serious impact on people's health; thus, all levels of government have implemented various pollution prevention measures since 2013. Based on multi-city in situ environmental and meteorological data, as well as the meteorological reanalysis dataset from 2013 to 2017, regional pollution characteristics and meteorological formation mechanisms were analyzed to provide a more comprehensive understanding of the evolution of $PM_{2.5}$ in NC. The domain-averaged $PM_{2.5}$ was 79 ± 17 μg m^{-3} from 2013 to 2017, with a decreasing rate of 10 μg m^{-3} yr^{-1}. Two automatic computer algorithms were established to identify 6 daily regional pollution types (DRPTs) and 48 persistent regional pollution events (PRPEs) over NC during 2014–2017. The average $PM_{2.5}$ concentration for the Large-Region-Pollution type (including the Large-Moderate-Region-Pollution and Large-Severe-Region-Pollution types) was 113 ± 40 μg m^{-3}, and more than half of Large-Region-Pollution days and PRPEs occurred in winter. The PRPEs in NC mainly developed from the area south of Hebei. The number of Large-Region-Pollution days decreased notably from 2014 to 2017, the annual number of days varying between 194 and 97 days, whereas a slight decline was observed in winter. In addition, the averaged $PM_{2.5}$ concentrations and the numbers and durations of the PRPEs decreased. Lamb-Jenkinson weather typing was used to reveal the impact of synoptic circulations on $PM_{2.5}$ across NC. Generally, the contributions of the variations in circulation to the reduction in $PM_{2.5}$ levels over NC between 2013 and 2017 were 64% and 45% in summer and winter, respectively. The three most highly polluted weather types were types C, S and E, with an average $PM_{2.5}$ concentration of 137 ± 40 μg m^{-3} in winter. Furthermore, three typical circulation dynamics were categorized in the peak stage of the PRPEs, namely, the southerly airflow pattern, the northerly airflow pattern and anticyclone pattern; the averaged relative humidity, recirculation index, wind speed and boundary layer height were 63%, 0.33, 2.0 m s^{-1} and 493 m, respectively. Our results imply that additional emission reduction measures should be implemented under unfavorable meteorological situations to attain ambient air quality standards in the future.

* Corresponding author at: State Key Laboratory of Atmospheric Boundary Layer Physics and Atmospheric Chemistry (LAPC), Institute of Atmospheric Physics, Chinese Academy of Sciences, Beijing 100029, China.
E-mail address: wll@mail.iap.ac.cn (L. Wang).
[1] These authors contributed equally to this work.

https://doi.org/10.1016/j.envint.2019.105283
Received 14 July 2019; Received in revised form 27 September 2019; Accepted 20 October 2019

1. Introduction

With the rapid pace of economic growth and urbanization, air pollution has become an increasingly serious issue in many developing countries. Both the government and the public are more concerned about air quality due to the adverse effects of particulate matter (PM) on human health, visibility and various climatic problems (Burnett et al., 2014; J. Li et al., 2016; Li, 2019; Z. Q. Li et al., 2016; Liao et al., 2015; Maji et al., 2018).

In recent years, air pollution episodes have been frequent in China, especially in the northern region (Cheng et al. 2016; Song et al. 2017; Wang et al. 2014c; Wang et al. 2014d; Zhao et al. 2016; Zheng et al. 2016; Zhu et al. 2016). To control the deteriorating situation, all levels of government have implemented various pollution prevention measures, e.g., the national-scale Action Plan for Air Pollution Prevention and Control issued in September 2013. Extensive studies have been carried out to investigate the characteristics and formation mechanisms of $PM_{2.5}$ (particulate matter with an aerodynamic diameter less than 2.5 μm) pollution over North China (NC). For example, $PM_{2.5}$ concentration and its chemical composition during the heavy haze pollution episode in January 2013 were analyzed (Huang et al. 2014; Wang et al. 2014d). Wang and Zhao (2018) compared the differences in $PM_{2.5}$ levels and their seasonal characteristics in 9 cities in the Beijing-Tianjin-Hebei (BTH) region. However, these studies focused on mainly individual pollution events or averaged conditions of the $PM_{2.5}$ concentration. Few studies focused on the evolutionary characteristics of daily regional pollution types (DRPTs) and persistent regional pollution events (PRPEs) in NC. To the best of our knowledge, only Tao et al. (2012) divided the daily regional pollution conditions into two groups (types Large and Partial) according to satellite observation, and persistent regional haze pollution events were identified based on the visibility and relative humidity in the period 1980–2013 (Wu et al. 2017). Therefore, to systematically understand the evolution of regional pollution under the condition of massive emission control measures implemented in recent years, more studies on regional pollution types and episodes in NC based on $PM_{2.5}$ data in multiple cities are required.

The severity of $PM_{2.5}$ pollution is known to be strongly dependent on emissions (Wang and Chen 2016; Zhang et al. 2012), topography (Wang et al. 2017), meteorology (Cai et al., 2017; Chen et al., 2018; Li et al., 2019), and physical and chemical reactions (Sun et al. 2015; Zhang et al. 2015). In particular, meteorological conditions are an important external factor that can affect the accumulation, diffusion and chemical progress of pollutants in a region. Therefore, synoptic and local meteorological conditions play an important role in causing air pollution.

Some studies have indicated a relationship between air pollution and synoptic circulation in NC. Typical circulation patterns and corresponding pollution levels and evolution processes have been analyzed by using a subjective circulation classification approach (Chen et al. 2008; Wang et al. 2014a; Wang et al. 2010; Wu et al. 2017; Zheng et al. 2015). In addition, objective weather classification methods have been applied extensively. Synoptic categorization techniques, such as the Kirchhofer method (Zhang et al. 2016), two-stage hierarchical clustering (Zhang et al., 2018a) and the T-mode method (Li et al., 2019; Ye et al., 2016), have been used to identify the most common circulation patterns in NC, with which different pollution levels have been connected with different synoptic circulation patterns. Local meteorological parameters (e.g., wind speed, mixing layer height, and humidity) related to $PM_{2.5}$ pollution have also been discussed. The dissipation of atmospheric particles depends mainly on the mixing layer height and wind speed (Tang et al. 2016; Wang et al. 2017; Zhu et al. 2018). Atmospheric humidity has a strong positive correlation with $PM_{2.5}$ concentrations, which has been attributed to an accelerated formation of particulate matter by physical and chemical processes during high moisture conditions (Leung et al. 2018; Sun et al. 2013; Zhu et al. 2016). In addition, recirculation corresponding to unfavorable ventilation has been shown to be one of the most important factors leading to heavy haze pollution events in BTH (Wang et al. 2014b; Ye et al. 2016). Noticeably, an investigation of regional pollution events elucidated that, following a thorough cleaning process, $PM_{2.5}$ concentrations in the central part of northern China (e.g., southern Hebei Province) could accumulate up to $> 100\ \mu g\ m^{-3}$ within 1–2 days under stagnant weather conditions, after which the region of high $PM_{2.5}$ concentrations could be extended over the whole NC and Yangtze River Delta through spatial oscillation and recirculation (Tao et al. 2016).

The aforementioned studies have comprehensively investigated the characteristics of individual pollution events and summarized the dominant weather types or meteorological conditions related to heavy air pollution. However, the statistics of weather types and the variation in key meteorological factors based on the evolution of persistent regional pollution episodes over NC are rarely investigated. In addition, the contribution of circulation changes to the interannual variability in $PM_{2.5}$ needs to be quantified so that the effect of emission control measures can be evaluated via separating the variability in long-term data due to climatological and environmental factors.

In this paper, we explore the variability in the characteristics and evolution of regional pollution types, as well as synoptic and local meteorological mechanisms over NC. The investigation is based on the daily $PM_{2.5}$ and meteorological data from 16 to 58 cities during 2013–2017. Our aims are (1) to characterize the variability in DRPTs and PRPEs over NC by developing automatic identification algorithms, (2) to conduct a quantitative analysis on the contribution of circulation changes to interannual variability in $PM_{2.5}$, and (3) to reveal the characteristics of synoptic weather types and circulation dynamics, as well as key meteorological factors (wind speed, relative humidity, boundary layer height, recirculation index, and precipitation) during different stages of persistent regional pollution episodes. These results are expected to provide important reference information for regional air pollution control.

2. Data

The NC provinces of Beijing, Tianjin, Hebei, Henan, Shanxi and Shandong are considered in this research (Fig. 1a). The data of the hourly concentrations of $PM_{2.5}$ were obtained for each station from the National Urban Air Quality Real-time Publishing Platform (http://106.37.208.233:20035/) issued by the Ministry of Ecology and Environment. First, daily averaged concentrations for each monitoring site were calculated based on the hourly data for the days with > 20 h of measurements, and then the daily mean value for all sites in one city were averaged as the daily average for that city (GB 3095-2012). $PM_{2.5}$ data were collected from 16 cities (133 sites) in 2013, from 42 cities (262 sites) in 2014 and from 58 cities (331 sites) in 2015–2017 (Table S1). Considering the heating period in the observed area, winter was considered the period between November 15th and March 15th. The other three seasons were defined here as follows: spring, March 16th to May 31st; summer, June 1st to August 31st; and autumn, September 1st to November 14th.

According to Fig. 1 and Table S1, the domain-averaged $PM_{2.5}$ concentrations were 79, 110, 68, 56 and 69 $\mu g\ m^{-3}$ during the whole year and in winter, spring, summer and autumn, respectively, and these concentrations decreased at rates of 10, 13, 7, 10 and 10 $\mu g\ m^{-3}\ yr^{-1}$. In addition, higher $PM_{2.5}$ concentrations and exceedance ratios (ERs) (the percentage of the days when the $PM_{2.5}$ concentration exceeded the Grade II National Ambient Air Quality Standard (NAAQS II) of 75 $\mu g\ m^{-3}$) were observed in southern Hebei in every season (Fig. 1c and d), which is associated with the dense population (Fig. 1b), highly concentrated industrial activity and special terrain in the piedmont plains (Fig. 1a).

Daily meteorological data, including relative humidity (RH), precipitation and wind speed (WS), for the 58 cities over NC were obtained

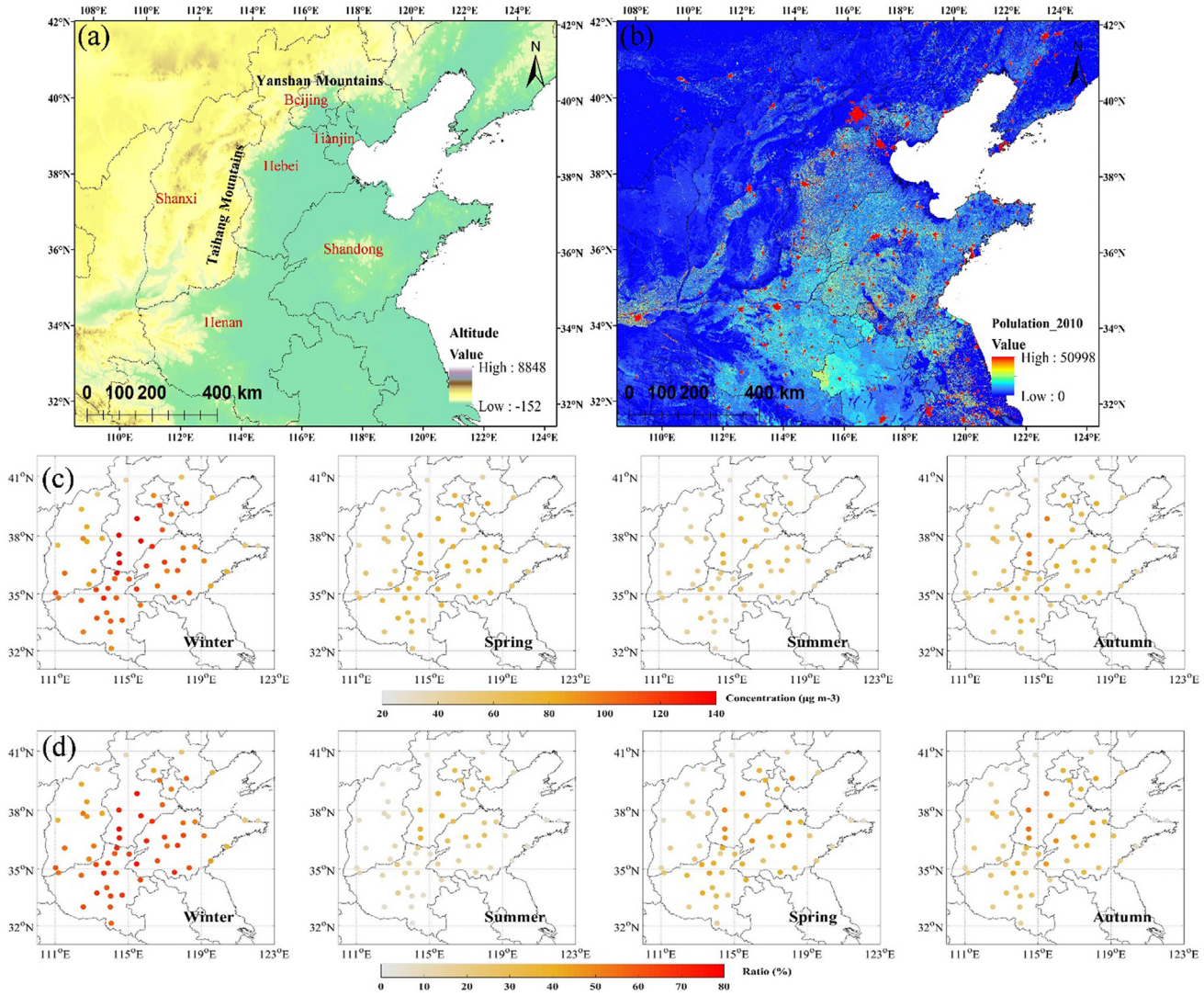

Fig. 1. Map of the study area and overview of regional pollution conditions. (a) Topographic map of NC; (b) population distribution map of NC; (c) averaged $PM_{2.5}$ concentration and (d) $PM_{2.5}$ exceedance ratios (ERs) for 58 cities in four seasons during 2013–2017.

from the National Meteorological Information Centre (http://data.cma.cn/). Eight measurements per day for were obtained for the U-wind and V-wind from the China Meteorological Administration in the Meteorological Information Combine Analysis and Process System (MICAPS). The 3-h interval (02:00, 05:00, 08:00, 11:00, 14:00, 15:00, 20:00, and 23:00 BJT) boundary layer height (BLH) (gridded at 0.25° × 0.25°), 6-h interval (02:00, 08:00, 14:00 and 20:00 BJT) sea level pressure (SLP), geopotential height at 500 hPa, wind vectors at 925 hPa, surface temperature, and surface dew-point temperature, WS, BLH, wind divergence and vertical velocity reanalysis data (gridded at 1° × 1°) were obtained from European Centre for Medium-Range Weather Forecasts (ECMWF) Re-analysis Interim (ERA-Interim).

3. Methods

3.1. Identifying DRPTs and defining PRPEs

Referring to the objective identification technique for regional extreme events (Ren et al. 2012), we developed a computer algorithm that can automatically identify DRPTs and then define PRPEs over the NC region based on $PM_{2.5}$ concentrations in 42–58 cities.

3.1.1. Identification of the DRPTs

A general flowchart to identify the DRPTs was developed (Fig. 2a). A polluted city (daily $PM_{2.5} > 75\ \mu g\ m^{-3}$), severely polluted city (daily $PM_{2.5} > 150\ \mu g\ m^{-3}$) and neighboring cities (any city j within 250 km) were defined first. The detailed analysis process is presented as follows:

(1) Define the daily regional pollution ratio R and the regional severe pollution ratio Rz. For each day, R = n/N, Rz = nz/N, where N, n, and nz represent the total number of regional cities, the number of polluted cities and the number of severely polluted cities, respectively. (2) Determine the neighboring pollution ratio. For each city, its neighboring pollution ratio r(j) is given by r(j) = x/X, where X and × are the number of neighboring cities and polluted cities, respectively. 3) Select the daily centers of regional pollution. Two conditions must be satisfied for these centers: r(j) > 0.4, and the distance between the centers is greater than 250 km. Every polluted city is scrutinized, and the daily regional pollution centers and their numbers are obtained. 4) Identify the pollution types. Based on the number of regional pollution centers (centern) and the values of R and Rz obtained above, six DRPTs are identified to reveal the daily regional pollution conditions: Clear, Local-Pollution (Local-P), Small-Region-Circle-Pollution (Small-C-P), Small-Region-Belt-Pollution (Small-B-P), Large-Moderate-Region-Pollution (Large-P), and Large-Severe-Region-Pollution (Large-S-P) (Table S2). Then, we combined Small-C-P, Small-

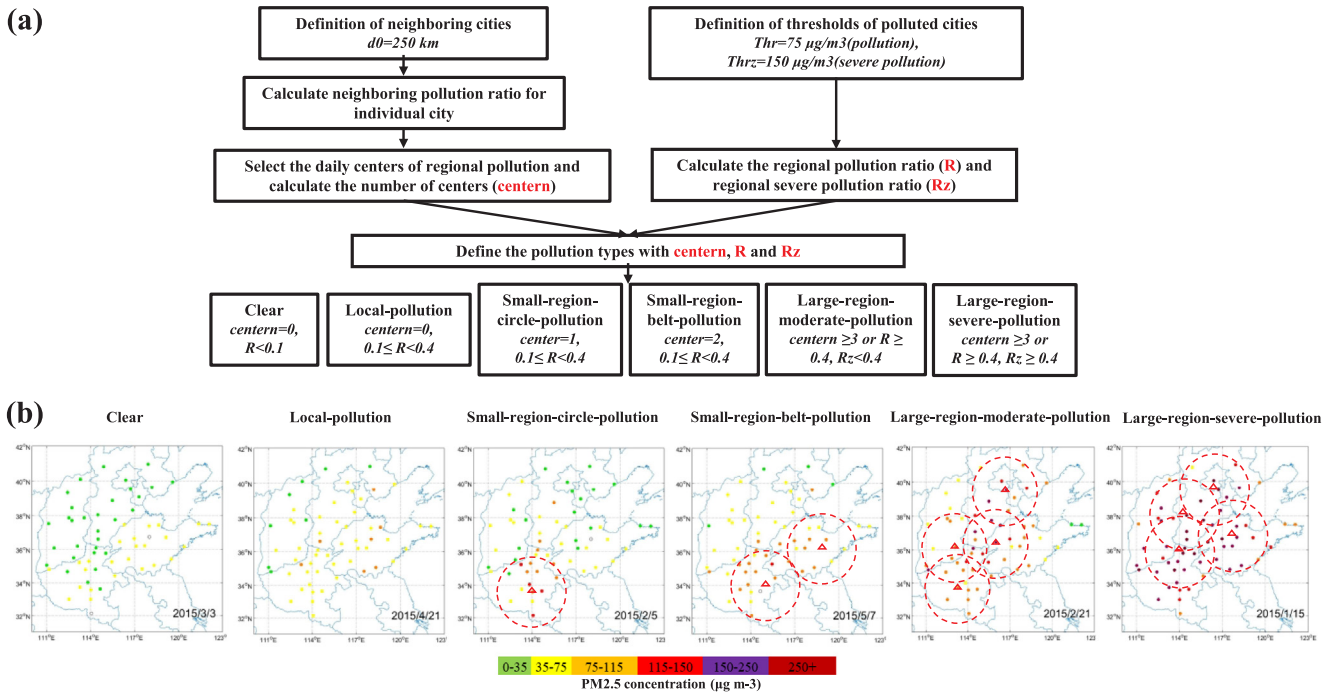

Fig. 2. (a) Flow chart for identifying DRPTs; (b) typical maps for 6 DRPTs.

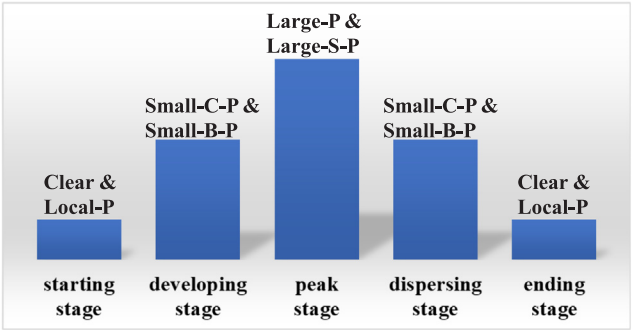

Fig. 3. The evolution stages of PRPEs.

B-P, Large-P and Large-S-P to create Region-P, Small-C-P and Small-B-P to create Small-Region-P, and Large-S-P and Large-P to create Large-Region-P. An additional criterion was added to help determine the type: If the number of centers < 3 and if R ≥ 0.4, manual correction of the DRPT is needed. The details of the identification are shown in Text S1, and typical maps for 6 DRPTs are depicted in Fig. 2b.

According to previous studies, regional events usually affect a certain domain and last for a specific time period (Andreadis et al. 2005; Ren et al. 2012). Therefore, DRPT identification is the basis of the definition of regional pollution events and can help to clarify not only the regional pollution variation characteristics in 2014–2017 but also the duration and starting area of persistent regional pollution over NC. The classification is not carried out in 2013 because the number of valid cities is not sufficient.

3.1.2. Definition of PRPEs

Wang et al. (2014d) proposed the definition of a haze episode at a station as two successive days with daily $PM_{2.5}$ exceeding 75 $\mu g\,m^{-3}$. Zheng et al. (2016) developed a program that could simultaneously divide haze episodes and identify their shapes. Here, a new algorithm for the automatic definition of regional pollution events is developed on the basis of the above studies in Section 3.1.1. With the input of a time series of DRPT, the algorithm program defines PRPEs via 3 major steps, as shown in Fig. S1. First, we identify periods in which the DRPT reaches Large-Region-P for at least 3 consecutive days as PRPE candidates; then, if some of the event candidates have no Clear and Local-P days between them, they will be combined into one event candidate that could reflect the oscillation of regional pollution; finally, we calculate the start/end days of the event candidates by searching forward/backward until Clear or Local-P days are found and obtain the complete events.

3.1.3. Definition of the evolution stages of PRPEs

The evolution of PRPEs in this study considers the entire event from start to end, with the evolution stages labeled in terms of the DRPT. We divided every regional pollution event obtained in Section 3.1.2 into five stages: a staring stage (Clear and Local-P), a developing stage (Small-C-P and Small-B-P), a peak stage (Large-P and Large-S-P), a dispersing stage (Small-C-P and Small-B-P), and an ending stage (Clear and Local-P Clean) (Fig. 3).

3.2. Lamb-Jenkinson weather typing

The automated Lamb-Jenkinson weather type (LWT) approach (Jones et al. 1993; Lamb 1972) was employed to classify the synoptic circulation patterns by describing the location of the high- and low-pressure centers that determine the direction of the geostrophic flow. Based on the gridded pressure data of a 16-point moveable region with a central area in the NC (Fig. S2a), the daily mean SLP data from four times (02:00, 08:00, 14:00 and 20:00 BJT) were used to determine the daily weather type during the period of 2013–2017. A small number of empirical rules devised previously (Jones et al. 1993; Trigo and DaCamara 2000) were then used to classify each day as one of the 26 weather types, consisting of two vorticity types (anticyclonic, A, and cyclonic, C); eight directional types (northeasterly, NE; easterly, E; southeasterly, SE; southerly, S; southwesterly, SW; westerly, W; northwesterly, NW; and northerly, N); and 16 hybrid types (CN, CNE, CE, CSE, CS, CSW, CW, CNW, AN, ANE, AE, ASE, AS, ASW, AW, and ANW, which are merged into one class named Others in this study because each type had only a few cases, which accounted for 0.66–4.3%, as shown in Fig. S2b). The mean surface pressure, wind

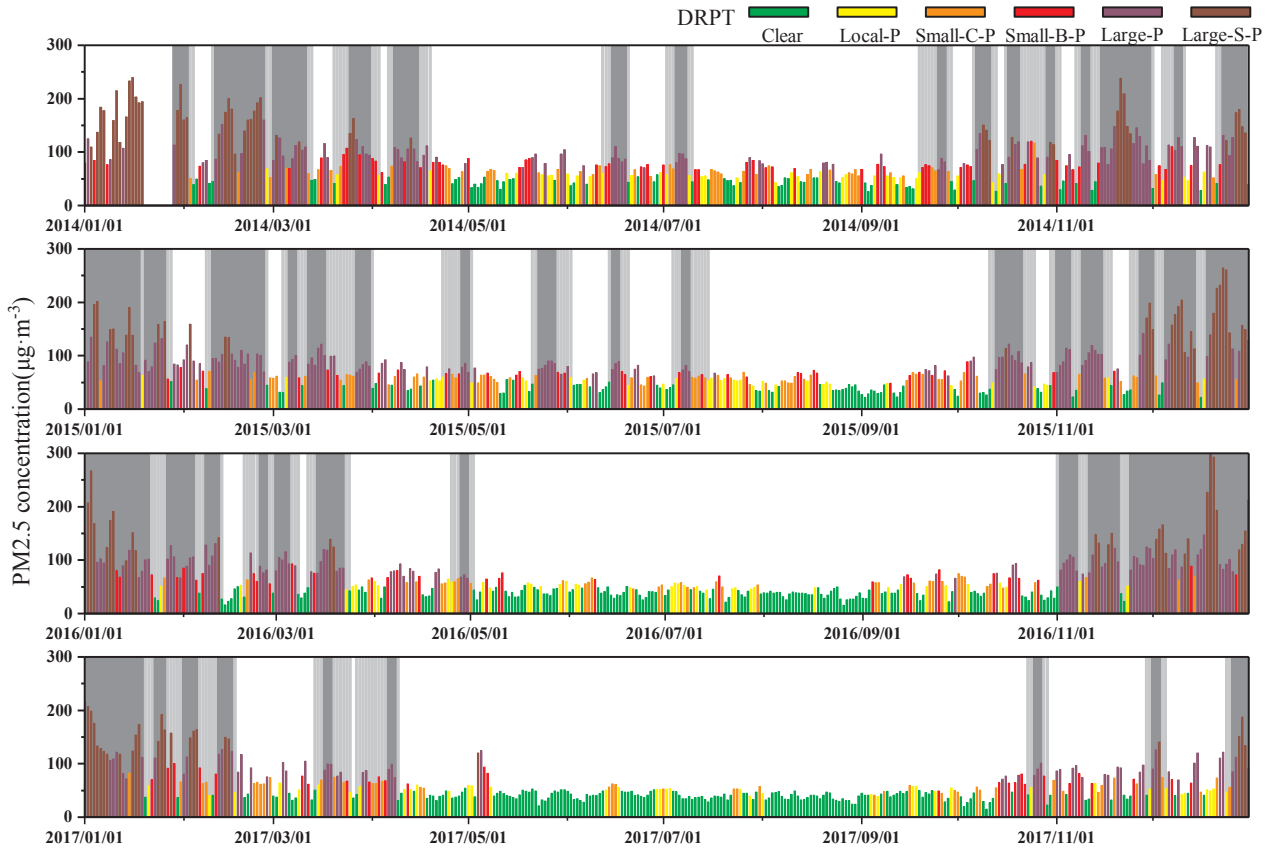

Fig. 4. Time series of daily domain-averaged concentrations of $PM_{2.5}$, DRPTs and PRPEs from 2014 to 2017. The height and the colors of the columns represent the domain-averaged values of $PM_{2.5}$ and DRPTs, respectively; PRPEs are shown in gray bands, and dark gray bands represent the peak stage during each event.

fields and occurrence days during 2013–2017 are shown in Fig. S2b for the 26 weather types. The eight directional types were able to reflect the dominant wind direction of the region, e.g. region was mainly affected by the southerly winds in type S.

3.3. Reconstruction of $PM_{2.5}$ concentration based on the synoptic classification

To quantify the interannual variability captured by synoptic circulations, Comrie and Yarnal (1992) suggested an algorithm to separate synoptic and nonsynoptic variability in environmental data by multiplying the overall mean value of a particular pattern by the occurrence frequency of that type of year. Hegarty et al. (2007) suggested that the variation in weather types was caused by both intensity and frequency changes in circulation and that the intensity change was the dominant factor. Hence, considering both the intensity and frequency of each circulation type, a reconstructed $PM_{2.5}$ concentration was described as follows:

$$\bar{PM}_{2.5m}(fre + int) = \sum_{k=1}^{26} (\bar{PM}_{2.5k} + \Delta PM_{2.5km})F_{km} \quad (1)$$

where $\bar{PM}_{2.5m}(fre + int)$ is the reconstructed mean $PM_{2.5}$ concentration influenced by the changes in frequency and intensity of the circulations in year m, and $\bar{PM}_{2.5k}$ and F_{km} are the 5-year mean original observed $PM_{2.5}$ concentration in weather type k and occurrence frequency of weather type k in year m, respectively. $\Delta PM_{2.5km}$ represents the part of the annual observed $PM_{2.5}$ oscillation caused by changes in the intensity of the circulations of each weather type, and it was obtained through a linear fitting of $PM_{2.5}$ annual anomalies ($\Delta PM_{2.5}$) based on the annual observed values and effective circulation intensity index (ECII) per weather type for the year m. Unlike in the method of Hegarty el al. (2007) (using only the domain-averaged SLP as ECII), 6 circulation intensity indexes were used to confirm the ECII for each weather type. The 6 circulation intensity indexes are (1) mean SLP; (2) the difference between the highest pressure and lowest pressure (gradient); (3)/(4) the center pressure of the highest/lowest pressure system; and (5)/(6) the distance from the highest/lowest pressure centers to the study city. Finally, the ECII per circulation is identified by the most relevant circulation intensity index with $\Delta PM_{2.5}$. All the indexes for 16 cities were calculated based on 10°×10° grids covering the domain 32°N-42°N, 110°E-120°E.

3.4. Recirculation index

To consider the characteristics of horizontal recirculation in each city, the recirculation index is defined based on the Allwine and Whiteman (1994) algorithm using a set of n discrete observations of U-wind and V-wind in a time period (τ, desired transport time, 24 h) within a time interval (T = 3 h). Three parameters were defined as follows:

$$L = T\left[\left(\sum_{i=1}^{n} u_i\right)^2 + \left(\sum_{i=1}^{n} v_i\right)^2\right]^{1/2} \quad (3)$$

$$S = T\sum_{i=1}^{n} (u_i^2 + v_i^2)^{1/2} \quad (4)$$

$$Rec = 1 - \frac{L}{S} \quad (5)$$

Here, Rec is the ratio of resultant transport distance (L) to scalar transport distance (S), which gives an indication of the presence of recirculation on time scales comparable to τ. If Rec equals one, no net

transport occurs, i.e., there has been a complete recirculation where the air parcel has returned to its origin, and a value of zero means a straight line (Allwine and Whiteman 1994; Ye et al. 2016).

Daily values of Rec were calculated for 42–58 cities using the three-hourly surface wind observations in 2014–2017. The calculations were regarded as invalid when less than 8 observations were available on a single day.

4. Results and discussion

4.1. Characteristics of DRPT and PRPEs

4.1.1. Characteristics of DRPTs

According to the method described in Section 3.1.1, the daily domain-averaged concentrations of $PM_{2.5}$, DRPTs number and ratios and averaged concentrations of DRPTs are shown in Fig. 4, Tables S2–S5. The domain-averaged concentrations for Clear, Local-P, Small-C-P, Small-B-P, Large-P, and Large-S-P were 39 ± 8, 53 ± 6, 60 ± 8, 73 ± 10, 94 ± 18 and 161 ± 39 $\mu g\,m^{-3}$, respectively. Overall, the total number of Clear days from 2014 to 2017 increased gradually, with 69, 78, 138 and 171 in 2014, 2015, 2016 and 2017, respectively. In contrast, Large-P days decreased notably, especially in 2017, varying from 101 days in 2016 to 69 days in 2017. Large-S-P days decrease sharply from 2014 to 2015 and then slowly from 32 in 2015 to 28 in 2017. These decreasing trends are attributed to the efficient emission control measures during the past several years and to the favorable meteorological conditions for dispersing pollutants, especially in 2017.

On a seasonal scale, Large-Region-P days were the main pollution types in winter, probably because of unfavorable synoptic conditions and residential heating (Chen et al. 2018; Zhang et al. 2012). More than 50% of the winter days were Large-Region-P days every year, and the daily domain-averaged concentrations of $PM_{2.5}$ during both Large-P and Large-S-P days were 100 ± 18 and 165 ± 40 $\mu g\,m^{-3}$, respectively. Remarkably, there was a slight increase in the number of Large-Region-P days in winter from 2014 to 2016, while a sharp decrease occurred in 2017 (Fig. 5). In contrast, the proportion of Large-Region-P days was mostly lower than 30% during the other seasons (Figs. 4 and 5).

Changes in the proportion of each pollution type presented almost the same trend in spring and autumn. The proportion of Large-Region-P days had a decreasing trend from 2015 to 2017, and the daily domain-averaged concentrations of $PM_{2.5}$ for Large-P days and Large-S-P days were similar in spring and autumn, at approximately 90 and 130 $\mu g\,m^{-3}$, respectively. However, Region-P was still the major pollution type in 2014 and 2015, between 60% and 75%. Meanwhile, the proportion of Clear days displayed a notable increase in these two seasons, representing more than half of the days in 2016 and 2017. The results showed that Clear days was the main regional pollution condition in spring and autumn in 2016 and 2017.

In summer, the region is dominated by Clear days. The proportion of Clear days was significantly higher than those in the other seasons. The number of Clear days in summer showed a remarkable increase from 41 days in 2014 to 85 days in 2017, with daily domain-averaged concentrations of $PM_{2.5}$ being below 45 $\mu g\,m^{-3}$ every year. The number of Region-P days decreased accordingly. In particular, no Large-Region-P days existed during the summer in 2016 and 2017; meanwhile, the proportions of Clear days were 84.8% and 92.4% in 2016 and 2017 (Tables S3–S5).

In general, the number and proportion of Clear days increased significantly in all the seasons from 2014 to 2017; the largest increase was observed in summer. However, Large-Region-P days had a significant downward trend from 2014 to 2017 except in winter, when a slight decrease occurred. Large-Region-P days decreased only 26% from 2014 to 2017 in winter, while the proportions were above 50% in other seasons. However, the corresponding domain-averaged concentrations of $PM_{2.5}$ for different DRPTs had small interannual variations of less than 10 $\mu g\,m^{-3}$ (Table S5).

4.1.2. Characteristics of PRPEs

Based on the algorithm described in Section 3.1.2, 48 PRPEs (64 candidates) were identified over NC during 2014 to 2017 (Fig. 4). The peak domain-averaged $PM_{2.5}$ concentrations of the events showed a downward trend, decreasing from 110 $\mu g\,m^{-3}$ in 2014 to 98 $\mu g\,m^{-3}$ in 2017; meantime, the $PM_{2.5}$ concentrations averaged over the whole events declined from 92 $\mu g\,m^{-3}$ (2014) to 74 $\mu g\,m^{-3}$ (2017). Notably, there was only a slight oscillation of averaged $PM_{2.5}$ concentrations during 2014–2016, whereas a sharp decline occurred in 2017. In addition, both the number and duration of regional pollution events decreased. The numbers of regional pollution events were 25 in winter, 10 in autumn, 9 in spring and 4 in summer, with more than half of the events occurring in winter. The duration time of these pollution events may reflect the persistence of unfavorable synoptic conditions. The trend of the average duration of the regional pollution events in different seasons followed that of the number of these events: 10.8 days in winter, 5.2 days in spring, 4.8 days in autumn and 3.8 days in summer (Fig. 6). Furthermore, 9 regional pollution events lasted for more than 10 days in winter, whereas none of the events lasted for more than 9 days in the other seasons. Remarkably, the regional pollution event

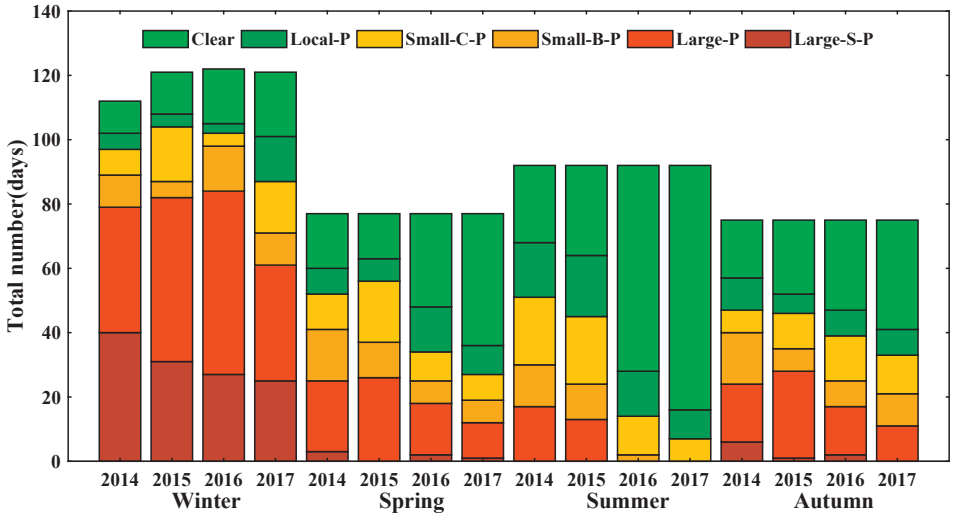

Fig. 5. The 6 DRPTs in the four seasons in 2014–2017.

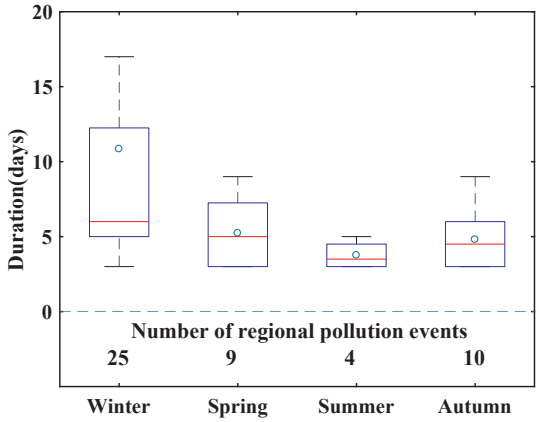

Fig. 6. Duration time of PRPEs in 2014–2017. The whisker and box show the minimum (maximum) value and 25% (75%) percentiles, respectively. The numbers under the dotted line represent the number of pollution events in each of the four seasons.

from November 24th, 2016, to January 16th, 2017, was the longest event in the study period, having a duration of 57 days. In addition, 9 of the 48 pollution events were combined events, reflecting the oscillation and continuity of regional pollution, indicating that the pollution in the whole region does not easily dissipate completely, especially in winter. Compared with the typical duration of pollution episodes of 3–5 days in Beijing (Zheng et al. 2016), the regional pollution events over NC clearly last much longer.

4.1.3. Starting areas of PRPEs

Th evolution of every regional pollution event was divided into 5 stages (Fig. 3). Fig. 7 displays the distribution of the frequency in every city where the daily concentration of $PM_{2.5}$ exceeded 75 $\mu g\,m^{-3}$ (NAAQS II) in the developing stage of different PRPEs. All 48 events and 9 oscillation events exhibited similar distribution characteristics. Clearly, the most frequently polluted cities are concentrated in the south of Hebei Province in the developing stage of the events (Fig. 7). In other words, the results indicated that the PRPEs in NC mainly start in southern Hebei. For the 48 events, 10 cities were acting at least 24 times as the starting centers of regional pollution events, with Baoding and Xingtai acting as many as 34 and 35 times, respectively. The reasons for this were large emissions of anthropogenic $PM_{2.5}$ and its precursors (Zhao et al. 2017) and unfavorable meteorological conditions for pollutant dispersion in these areas, including extremely low wind speeds (Tao et al. 2016; Wang et al. 2014b). The high concentrations of pollutants in southern Hebei could be transported into the surrounding areas via the wind, increasing pollution levels in NC to some extent. Therefore, strengthening pollution control in southern Hebei is very important for reducing pollution concentrations in the whole NC region.

4.2. Analysis of meteorological causes of regional pollution

4.2.1. Relationship between weather types and regional $PM_{2.5}$ pollution

Weather types are thought to be closely related to air quality (Zhang et al., 2016, 2018). In this study, 26 weather types over NC were identified using the LWT approach discussed in Section 3.2, and 11 types were combined (Fig. 8) to analyze the regional circulation situations and corresponding $PM_{2.5}$ concentrations and DRPT characteristics.

As shown in Fig. 8a, type A (44.1%), eastern types (30.0%, types E, NE, SE and ANE were being most common), and Others (29.9%, types AN, ANE and AE being the most common) were the dominant weather types in winter. The predominant types in autumn were type A (36.3%) and Others (23.7%, types AN, ANE, AE and ASW being most common). In spring, type A (15.9%) and Others (24.4%, types ANW, ASW and CSW being most common) as well as western circulation (32.0%, SW, W, NW, ASW and ANW) were predominant. Summer showed a very different circulation distribution, with the lowest fraction of type A (8.2%) but the highest fraction of type C (33.4%), while types CN, CNE and CNW were the most common in the Others category, which reflects that cyclone circulation occurred frequently during this season.

Fig. 8b reveals that winter had the highest domain-averaged $PM_{2.5}$ concentration of above 85 $\mu g\,m^{-3}$ for all the weather types, whereas the lowest concentrations (52 $\mu g\,m^{-3}$ on average for all weather types) were observed in summer. For the four seasons in general, the highly polluted types were mainly related to C, southern (types S, SE, and SW) and eastern (type E) circulations, whereas the less polluted types were mainly related to A, northern (type N) and western circulations (type W). However, the relationships between domain-averaged $PM_{2.5}$ concentrations and the 11 weather types in the four seasons showed little differences.

In winter, the two highest $PM_{2.5}$ circulations were type S and E (both 125 $\mu g\,m^{-3}$ on average), followed by type C (124 $\mu g\,m^{-3}$). S and E circulations are conducive to the transport and accumulation of pollutants from the south plain, resulting in higher $PM_{2.5}$ concentrations because southerly or easterly winds prevail (Wang et al., 2014b). In addition, the region is mainly dominated by southerly wind in type C (Fig. S2b). The WSs of types S and SE were lower than 2 $m\,s^{-1}$, and the two highest RH circulations in winter corresponded to types SE and E

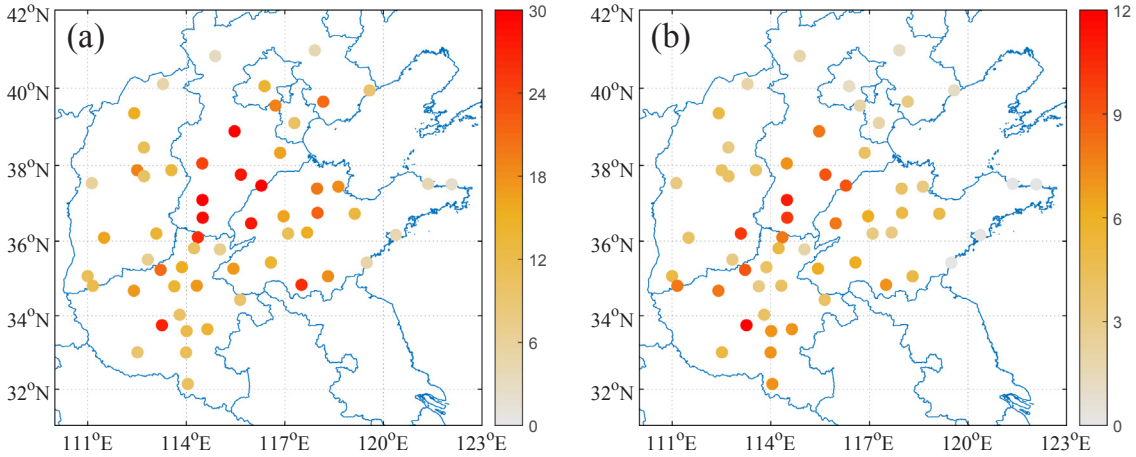

Fig. 7. (a) and (b) Distribution of the frequency in every city where the daily $PM_{2.5}$ concentration exceeded the NAAQS II in the developing stage during the 48 PRPEs and 9 oscillatory PRPEs, respectively. The NAAQS II is 75 $\mu g\,m^{-3}$.

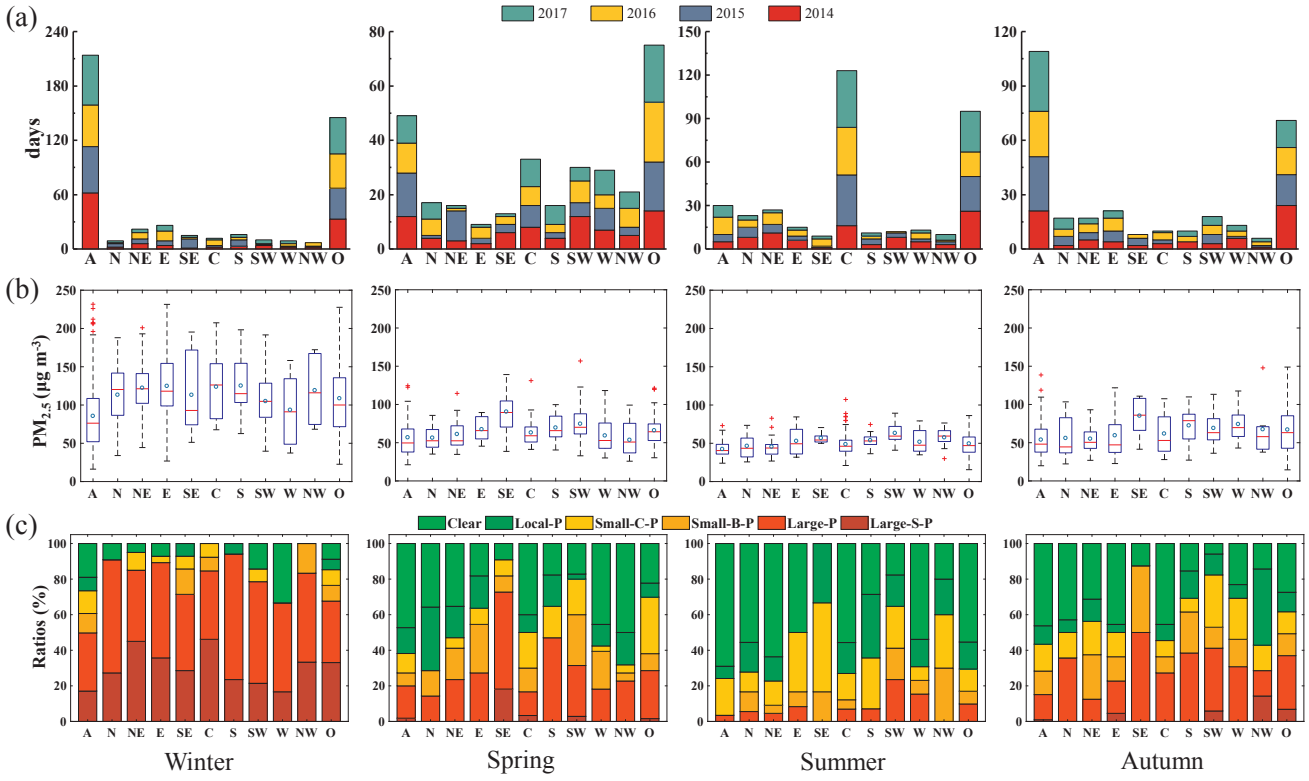

Fig. 8. (a) Number of days; (b) box charts of $PM_{2.5}$ concentrations; and (c) the ratio of DRPTs for every weather type in each of the four seasons during 2014–2017. Type O (Others) represents the merged 16 hybrid types (CN, CNE, CE, CSE, CS, CSW, CW, CNW, AN, ANE, AE, ASE, AS, ASW, AW, and ANW). The percentiles of the box and whisker plots in (b) are consistent with those in Fig. 6.

(the RH was greater than 60% on average) (Fig. S3). The results indicated that the lower WS and higher RH caused by southern, eastern or cyclone circulations were favorable for increasing $PM_{2.5}$. This is consistent with the findings of previous studies (Ma et al., 2017; Zhang et al., 2016, 2018a). The proportion of days reaching the Region-P (including Small-C-P, Small-B-P, Large-P and Large-S-P) level was more than 80% in winter (Table S3), so there was little difference among the proportions of Region-P days of the different weather types (Fig. 8c). Notably, the two least-polluted types in winter were types A and W; the number of Clear and Local-P days were relatively high, and the domain-averaged concentrations were both 95 $\mu g\,m^{-3}$. High pressure, generally under anticyclone circulations, corresponds to the removal process because the region is dominated by northerly wind (Fig. S2b). However, the lower WSs in type A could also sometimes lead to severe regional pollution.

Type SE had the highest domain-averaged concentrations in both spring (90 $\mu g\,m^{-3}$) and autumn (85 $\mu g\,m^{-3}$), and the corresponding proportions of Region-P days were large (90.9% and 87.5%, respectively). Similar features were present in types S and type SW. Therefore, under the influence of southerly winds, regional $PM_{2.5}$ concentrations tend to reach high levels. In contrast, type NW and type A had the lowest concentrations in spring and autumn, averaging 54 $\mu g\,m^{-3}$.

In summer, because the ratios of Clear days were significantly higher than those in other seasons (Table S3) and the proportions of Large-Region-P days were under 10% (except for types SW and W) per weather type (Fig. 8c), the regional average $PM_{2.5}$ concentrations were all lower than 65 $\mu g\,m^{-3}$ (Fig. 8b). Abundant precipitation and less anthropogenic emissions were the main reasons for the lower pollution levels in summer compared with those in other seasons.

4.2.2. Quantifying the effects of weather changes on the interannual $PM_{2.5}$ variations

The concentrations of $PM_{2.5}$ are tightly linked with meteorological conditions, as demonstrated by the analysis conducted above. An unfavorable synoptic circulation pattern exacerbates air pollution levels in the presence of a high emission background (Liao et al. 2018; Wang et al. 2017). To quantify the contribution of changing meteorological conditions on interannual variability in $PM_{2.5}$ over NC, we reconstructed $PM_{2.5}$ concentrations in 16 cities from 2013 to 2017 with a method that relies on Eq. (1). The meteorological contributions were approximated as the ratio of the following two metrics in each city: (1) the difference between the maximum and minimum reconstructed $PM_{2.5}$ concentrations and (2) the difference in observed $PM_{2.5}$ concentrations in these 5 years. The annual averaged values of observed $PM_{2.5}$ and reconstructed $PM_{2.5}$ in the four seasons are shown for each city in Table S6. In general, the contributions of interannual variability to $PM_{2.5}$ as influenced by the variation in circulations ranged from 40% to 65% annually in the 16 cities (Table 1), which reflects changes in the frequency and intensity of circulations resulting in interannual fluctuations in $PM_{2.5}$ concentrations. The contributions of the variations in circulation in spring and summer (city-averaged contributions of 59%) were higher than those in autumn and winter (45%).

Based on the interannual seasonal variability in domain-averaged $PM_{2.5}$ over the 16 cities, the maximum values (80, 100, and 146 $\mu g\,m^{-3}$ in summer, autumn and winter, respectively) were observed in 2013, and minimum values (45, 58, and 88 $\mu g\,m^{-3}$, respectively) were observed in 2017, spring being an exception to this pattern, which indicated that $PM_{2.5}$ levels were 44%, 42% and 40% lower in 2017 than in 2013, respectively. The contributions of variations in circulation on the total reduction in $PM_{2.5}$ were 64%, 58% and 45% in summer, autumn and winter, respectively, in those 2 years. The remaining interannual variability was possibly due to nonlinear emission reductions recently conducted over NC. The results indicate that the meteorological contribution to the interannual $PM_{2.5}$ reduction was higher in summer than in winter.

Table 1
Contribution of weather changes to $PM_{2.5}$ interannual variation in 16 cities in the four seasons.

City Name	Spring	Summer	Autumn	Winter	All
Chengde	66.0%	71.6%	29.6%	60.0%	55.7%
Zhangjiakou	78.4%	56.8%	32.7%	45.2%	56.0%
Beijing	76.0%	58.8%	61.3%	72.9%	65.4%
Qinghuangdao	48.3%	54.7%	39.5%	44.5%	47.5%
Tangshan	51.4%	64.4%	23.8%	51.6%	46.5%
Langfang	36.3%	58.9%	24.9%	46.3%	40.1%
Tianjin	56.6%	59.7%	42.1%	33.8%	52.8%
Baoding	78.3%	63.6%	42.2%	44.6%	61.4%
Cangzhou	46.8%	55.0%	38.2%	34.5%	46.7%
Shijiazhuang	50.2%	56.4%	52.3%	52.6%	53.0%
Taiyuan	58.9%	67.7%	57.6%	62.6%	61.4%
Hengshui	81.0%	56.1%	50.5%	35.2%	62.5%
Xingtai	55.4%	58.4%	53.8%	45.4%	55.9%
Jinan	44.1%	48.8%	37.0%	50.1%	43.3%
Handan	48.2%	60.5%	39.2%	24.1%	49.3%
Zhengzhou	50.4%	65.4%	38.5%	84.5%	51.5%

Note: The contributions in the table were the ratio of the difference between maximum and minimum for reconstructed $PM_{2.5}$ oncentration and the difference for observed $PM_{2.5}$ concentration. The weather change is associated with the change in the frequency and intensity of the circulations.

4.2.3. Characteristics of synoptic types and key meteorological factors based on PRPEs evolution

For a better understanding of the meteorological influence on PRPEs, Fig. 9 shows the fraction of weather types in different stages during regional pollution events. For all 48 PRPEs, the number days belonging to the starting stage, developing stage, peak stage, dispersing stage and ending stage were 58, 54, 381, 44 and 54, respectively. Type A was the dominant circulation in the starting stage, with a proportion of 63.8%, followed by Others (types AN and AS were most common). Additionally, in the developing stage, type A and Others also had the largest proportions, whereas the proportion of southwestern circulations (types ASW and SW) had a notable increase from the starting stage. In the peak stage, the Others (31.5%, types ANE, AE, ASE, AS and ASW were most common), southern (16.0%, including type S, SW and SE) and eastern (10.5%, including types E and SE) circulations types were dominant, which reflects pollutant transportation and abundant vapor from the south and east regions. In contrast, northern circulation (types N and NE) was rare, at 5.5%. Anticyclone-related (types ANE and AN were dominant in Others), and northern (types W, N and NE) circulations began to increase when evolving into the dispersing stage. Notably, type C increased significantly, which was associated with a frontal passage. In the ending stage, type A and the northern (types N, NE, AN and ANE) types were more frequent than they were in the developing or dispersing stage, which provides favorable synoptic conditions for pollutant dispersion. The proportion of weather types during the 25 air pollution events in winter is displayed in Fig. S4. Generally, the circulation features during the winter pollution events were in accordance with those during all the events, whereas the proportion of type A was higher because of frequent cold airflows in winter. Consequently, type A circulation days clearly decreased, while southern (types S and SW) and eastern (types E and SE) circulation days increased from the starting stage to the peak stage. The number of anticyclone-related and northern (type N) circulation days increased from the peak stage to the ending stage.

Not only weather types but also meteorological factors exhibit crucial links to pollution events. According to Fig. 10, the key parameters of RH, WS, BLH and Rec displayed remarkable regularity during the evolution of all the PRPEs. In general, RH and Rec first increased and then decreased gradually from the starting stage to the ending stage, while WS and BLH exhibited the opposite trend. From the starting stage to the peak stage, the averaged RH notably increased from 49 ± 17% to 63 ± 10%. Moreover, WS decreased from 2.4 ± 0.7 m s^{-1} in the starting stage to 2.0 ± 0.3 m s^{-1} in the peak stage, and BLH decreased from 618 ± 207 m to 493 ± 177 m, respectively. Despite the maximum value of Rec (0.35) occurring in the developing stage, the value of Rec in the peak stage (0.33 ± 0.06) slightly increased from that in the starting stage (0.31 ± 0.11), indicating that the recirculation capacity of air parcel increased with the development of pollution. Furthermore, the high RH and Rec values together with the low WS and BLH values were in accordance with southern- and eastern-related circulation in the peak stage, as shown in Fig. 10. In this comparison, RH decreased from 63 ± 10% to 53 ± 19% in the dispersing process. Recirculation gradually weakened during the dispersion stage, with Rec reducing by 27%, whereas both BLH and WS increased dramatically (41% BLH and 43% WS, respectively). Furthermore, Fig. S5 illustrates that in the peak stage in winter, a higher Rec and lower BLH occurred with values of 0.34 ± 0.07 and 404 ± 129 m, respectively. In addition, the averaged RH and WS were 59 ± 9% and 2.0 ± 0.3 m s^{-1}.

The regional distribution of four meteorological parameters (Fig. 11) could reflect the evolution of PRPEs for different cities. The RH in the south of the region was higher than that in the north, while

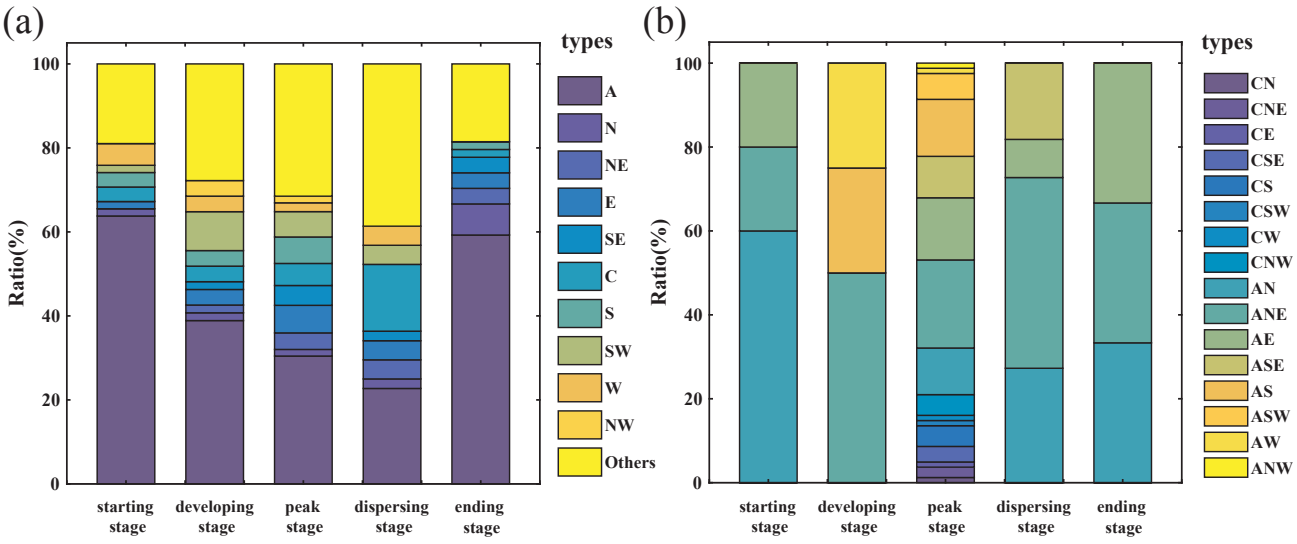

Fig. 9. (a) Ratio of weather types in every evolution stage for all PRPEs. (b) Ratio of weather types for Others in every evolution stage for all PRPEs. Others represents the merged 16 hybrid types (CN, CNE, CE, CSE, CS, CSW, CW, CNW, AN, ANE, AE, ASE, AS, ASW, AW, and ANW).

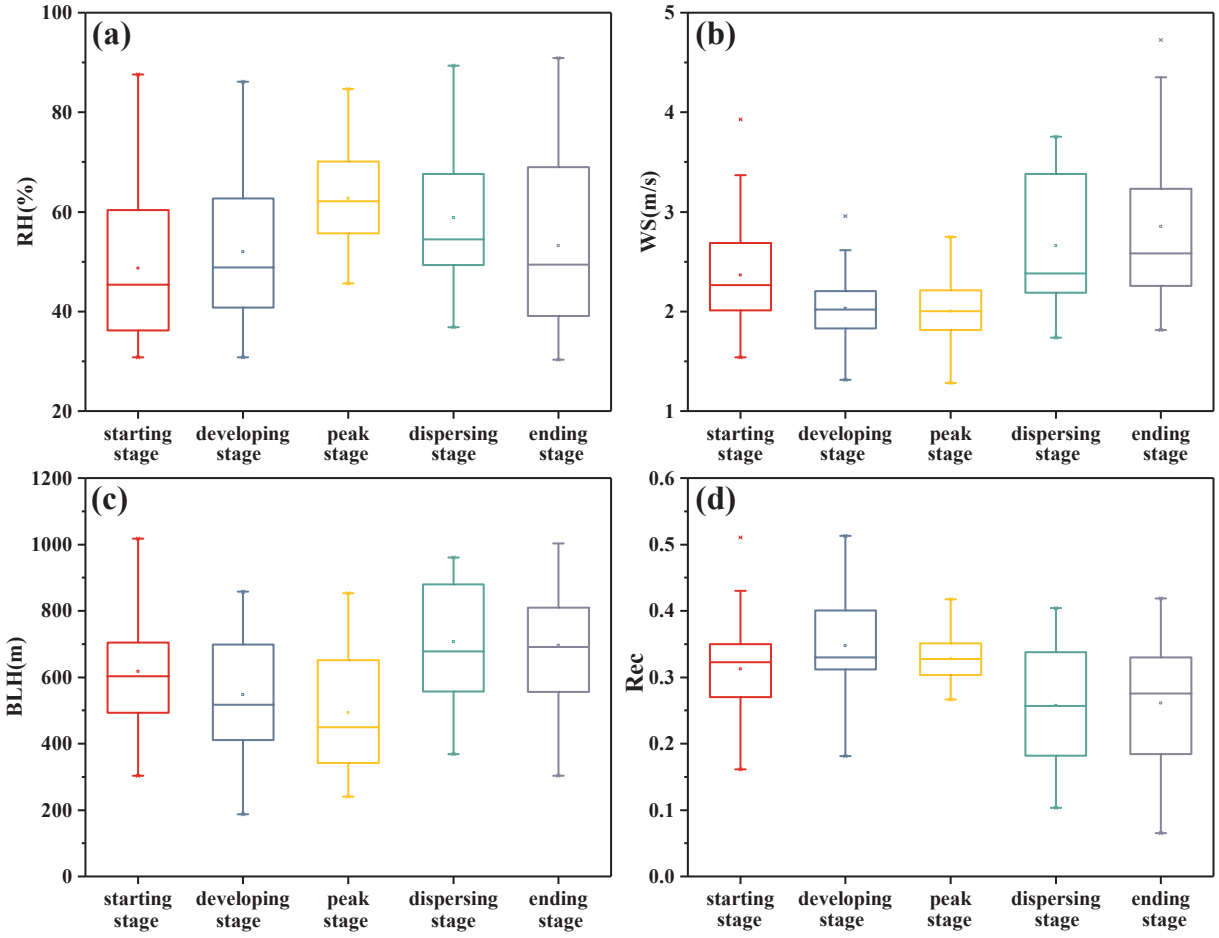

Fig. 10. Variations for key meteorological factors in every evolution stage for all PRPEs. RH, WS, BLH, and Rec represent the relative humidity, wind speed, boundary layer height, and recirculation index, respectively. The percentiles of the box and whisker plots are consistent with those in Fig. 6.

the difference tended to be smaller with the development of events. Most likely affected by the southerly airflow, RH underwent a sharp increase in the central area in the peak stage, which was comparable to that in the south. During the dispersing stage, RH in the north quickly decreased to approximately 50%, which was associated with cold and dry air from the northwest. At the same time, RH in the southern area decreased gradually. The variation in BLH was similar to that in RH during the regional events. BLH in the central and southern NC first declined as the events unfolded, until the peak stage was reached. The regional BLH was lower than 500 m overall, and the minimum BLH among all the cities decreased to 394 m in the peak stage. Moreover, the differences in BLH among cities were not large. From the northwest to the southeast of the region, the BLH rapidly rose to more than 650 m in the dispersing process of the events. This result illustrated that northern-related synoptic circulations played a key role in regional pollution removal. WS varied between 2.0 and 3.0 m s^{-1} in most cities, except for several cities located in the northern area and east coast. The minimum regional value of WS was observed at the peak stage, in accordance with the result shown in Fig. 11. Rec reached its maximum in the peak stage and then decreased slightly throughout the region. The western region (Shan Xi Province) and middle region (south of He Bei Province) had higher values of Rec than the other areas of NC during the evolution of the studied events, which could be related to the differences in terrain. The regional events in winter exhibited a similar regional distribution of meteorological characteristics, as shown in Fig. S6. In particular, the regional BLH was lower in the peak stage in winter, and the BLH in most cities was below 450 m. In addition, RH decreased more quickly during the winter dispersing stage.

4.2.4. Meteorological dynamic mechanism of the PRPEs during the peak stage

The peak stage is the most important period during the PRPEs. The number of days in the peak stage was 252 in winter, followed by 51, 45 and 15 in autumn, spring and summer, respectively, from 2014 to 2017 (Table S7). As analyzed in Section 4.1.2, more than half of the regional pollution events with longer durations occurred in winter, so that the great majority of days in the peak stage were in winter. In particular, 89% (108 of 122) of the Large-S-P days were in winter. In addition, the average $PM_{2.5}$ concentration (129 ± 43 μg m^{-3}) in the winter peak stage days was the highest, and the BLH (380 ± 154 m) in winter was the lowest among the four seasons. Small differences were reflected in RH, WS and Rec in the four seasons, but all showed high RH, weak wind and strong recirculation.

We explored atmospheric circulation and dynamic mechanisms during the peak stage in different seasons by analyzing the characteristics of the three-dimensional structure of atmospheric circulation at different levels in the troposphere and the spatial distributions of key meteorological factors (Fig. 12, Table 2, Figs. S7–S9, and Table S7). According to the large-scale circulations in different levels and the 26 weather types identified by the LWT approach, three specific circulation dynamics can be categorized, namely, the southerly airflow pattern, the northerly airflow pattern and the anticyclone pattern.

The circulation conditions in winter were used as examples to illustrate the characteristics of these three major circulation patterns. Fig. 12 depicts composite distributions of the $PM_{2.5}$ concentration, geopotential height at 500 hPa, SLP, wind fields at 925 hPa, surface RH, surface WS and BLH in three typical circulation patterns in the peak

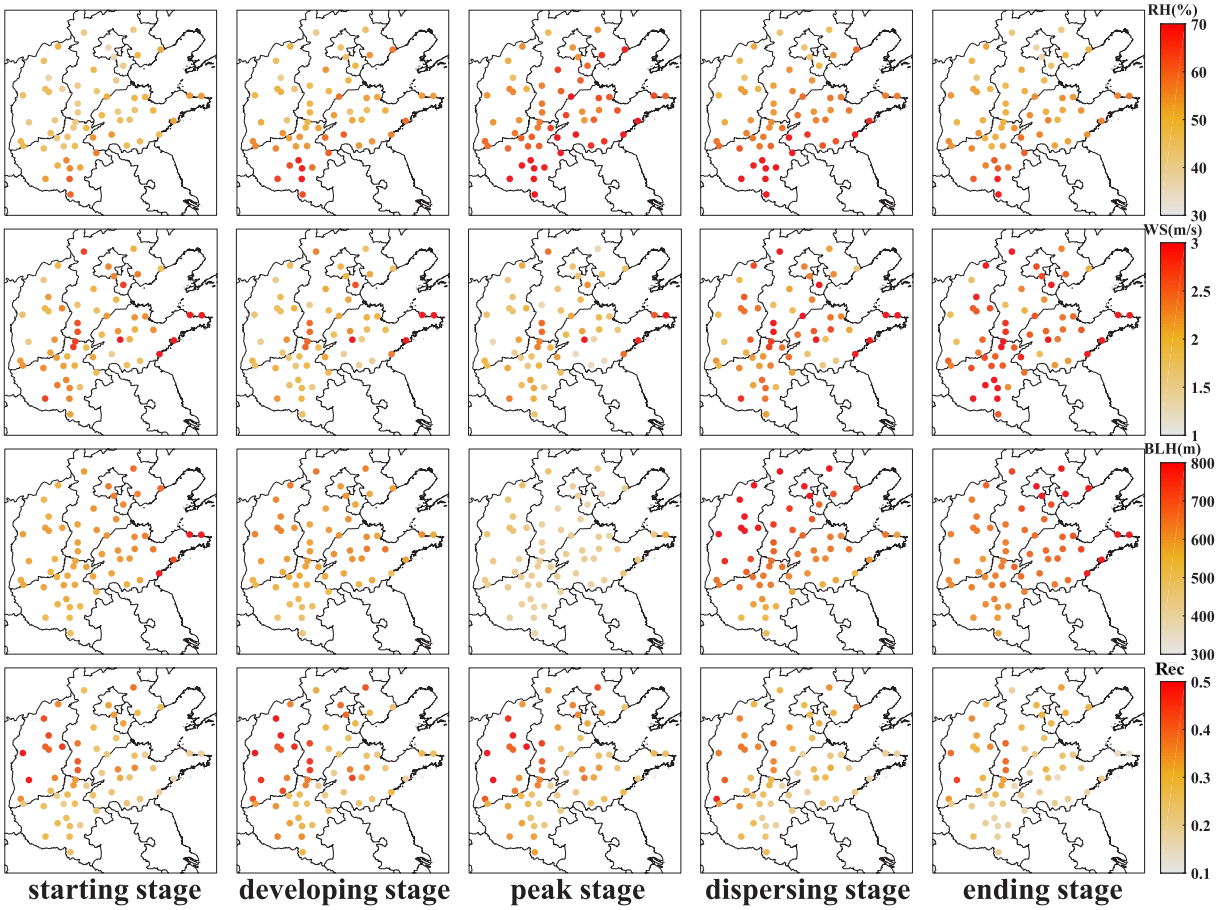

Fig. 11. Regional distribution of key meteorological factors in each evolution stage for all the PRPEs.

stage during PRPEs in winter. When the southerly airflow pattern occurred, NC was mainly dominated by zonal westerly or northwesterly airflow in the middle troposphere (500 hPa) and southwesterly or southeasterly winds in the low troposphere (925 hPa), which could bring warm and humid airflows from the southern area and aggravate regional pollution. The highest $PM_{2.5}$ concentration was shown in the plain in front of the Taihang Mountain due to the accumulation of pollutants caused by weak southerly winds. There was a weak pressure gradient at the surface, with a low WS of 1.0–2.5 m s^{-1} and a high RH of 50% to 80%. BLHs were very low in the region and varied from 200 to 400 m. When the northerly airflow pattern occurred, the NC region was controlled by zonal westerly or northwesterly airflow in the middle troposphere and weak northerly winds in the low troposphere, indicating less cold and dry air intrusion from high latitudes into the region. The NC region showed a weak pressure gradient at the surface, and the WS and BLH over NC were lower than 3.0 m s^{-1} and 500 m. When the anticyclone pattern occurred, zonal northwesterly airflow and anticyclone circulation prevailed over the NC region at 500 hPa and 925 hPa, respectively. The region was controlled by a uniform pressure field at the surface. At this time, the RHs over NC was higher, varying from 50% to 80%, and BLH and WS were both low. The $PM_{2.5}$ concentrations in three typical circulation patterns for all the cities were higher than 100 μg m^{-3} (Fig. 12a). Generally, the three circulation dynamics in the other seasons exhibited similar characteristics, as shown in Figs. S7–S9. In addition to horizontal motion, vertical motion is an important dynamic factor for the PRPEs. When the three patterns occurred, the wind almost presented a divergence in the mid-lower troposphere, except for a shallow convergence near the surface in the southerly airflow pattern. Moreover, downward winds were shown at 1000–500 hPa in each pattern (Fig. 12e). The result indicated that the NC region was completely controlled by a sinking motion in the mid-lower troposphere during PRPEs in winter. The region was also dominated by a sinking motion in spring (Fig. S7), but some ascending motions were shown during PRPEs in summer and autumn (Figs. S8 and S9).

Generally, most days of the peak stage could be classified in terms of the three typical meteorological dynamic mechanism patterns (Table S7). In winter, the numbers of days with the southerly airflow pattern, the northerly airflow pattern and anticyclone pattern were 45, 78 and 119 days, respectively; and 16, 40 and 48 days of the three circulation patterns reached Large-S-P, respectively, which indicated that large severe pollution events more easily occurred under the northerly airflow pattern and anticyclone pattern. The peak stage days in spring and autumn were dominated by the southerly airflow pattern and anticyclone pattern, and the days in summer were dominated by the southerly airflow pattern (Table S7).

4.2.5. *The effect of wet and dry removal on PRPEs*

The effects of wet and dry removal on regional pollution events were analyzed based on precipitation and wind speed data of 58 cities in different dispersing processes (Fig. 13). In this study, there are two dispersing processes considered for regional pollution. One was named the Slow-Removal process, i.e., the dispersing process from the peak stage, through the dispersing stage, and ending in the ending stage. In contrast, the regional pollution that was dispersed directly from the peak stage to the ending stage was named Rapid-Removal. We used the averaged wind speed in dispersing process to describe dry removal. The average wind speed of 58 cities in the Slow-Removal process (2.4 m s^{-1}) was lower than that in the Rapid-Removal process (2.6 m s^{-1}), which reflected that regional events could scavenge more

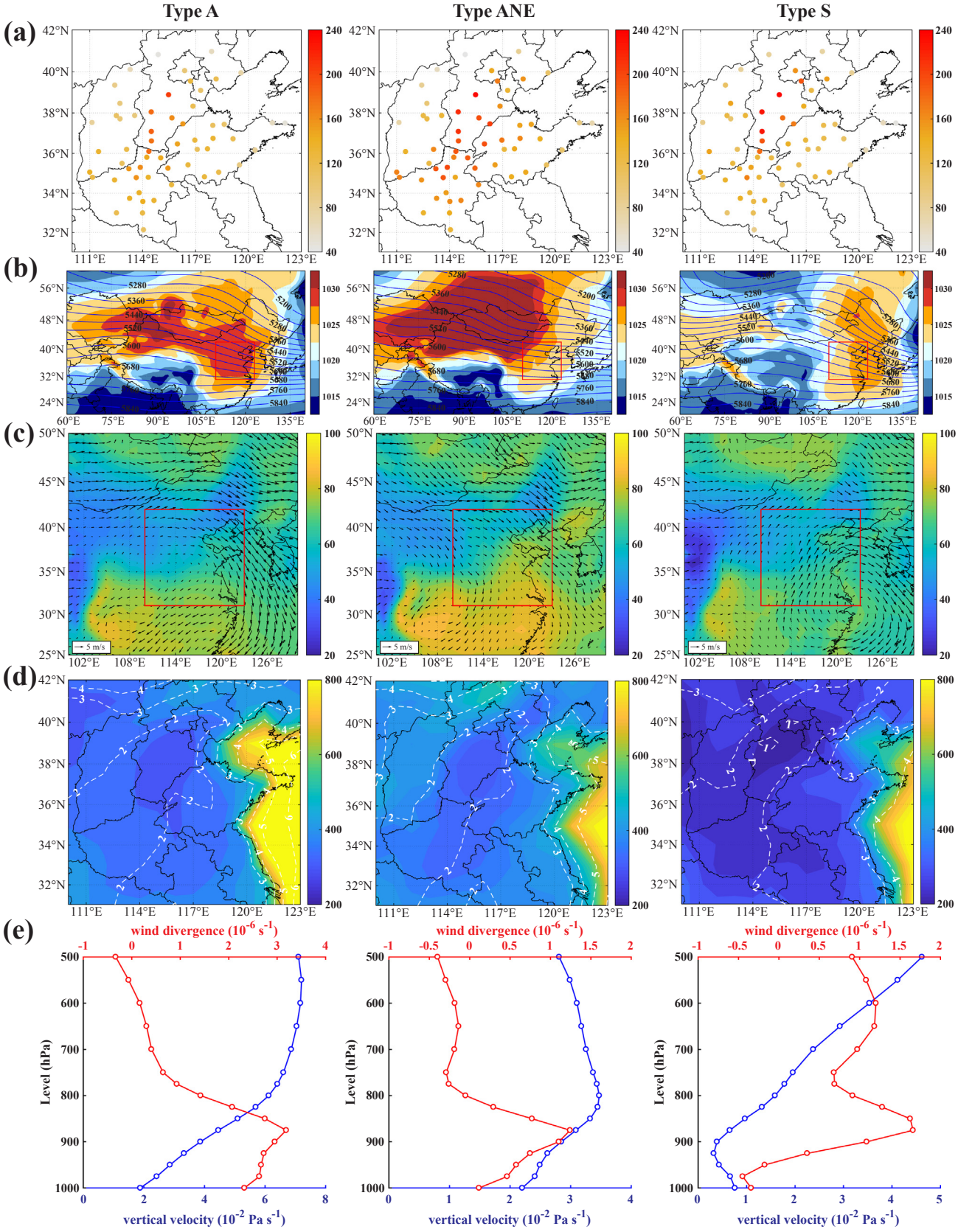

Fig. 12. Composite distributions of environmental and meteorological factors in three typical circulation dynamics in winter. (a) $PM_{2.5}$ concentration (units: μg m^{-3}); (b) geopotential height at 500 hPa (units: gpm) and SLP (shading; units: hPa); (c) wind fields at 925 hPa (vectors) and surface RH (shading; units: %); (d) surface WS (dashed line; units: m s^{-1}) and BLH (shading; units: m); (e) vertical distribution of wind divergence (red line; units: 10^{-6} s^{-1}) and vertical velocity (blue line; units: 10^{-2} Pa s^{-1}). (For interpretation of the references to colour in this figure legend, the reader is referred to the web version of this article.)

Table 2
Averaged values of key meteorological factors in the peak stage for all the PRPEs in the four seasons.

Season	PM2.5 (μg m^{-3})	RH (%)	WS (m s^{-1})	Rec	BLH (m)
Winter	129 ± 43	62 ± 13	2.0 ± 0.5	0.34 ± 0.08	380 ± 154
Spring	95 ± 21	60 ± 9	2.3 ± 0.5	0.3 ± 0.08	692 ± 120
Summer	83 ± 9	67 ± 5	1.9 ± 0.2	0.33 ± 0.06	769 ± 89
Autumn	102 ± 19	72 ± 9	1.8 ± 0.4	0.31 ± 0.06	407 ± 95

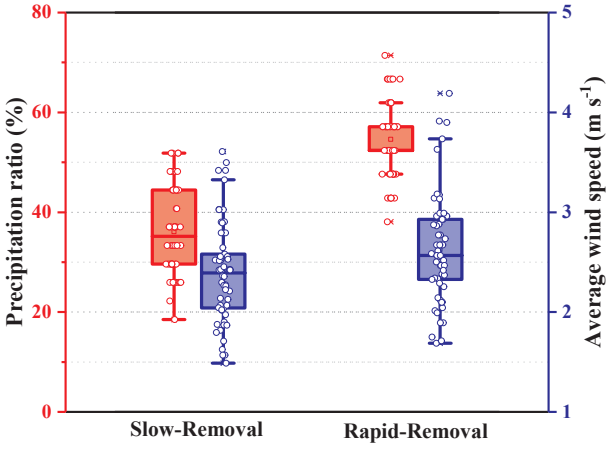

Fig. 13. Variations for precipitation and wind speeds in different dispersing processes for 48 PRPEs. The dispersing processes included the Slow-Removal process, representing the evolution from the peak stage to the dispersing stage, and the Rapid-Removal process, representing the evolution from the peak stage directly to the ending stage. Red box (left): Precipitation ratio represents the ratio of the number of events with precipitation to 48 events in different dispersing processes per city. Blue box (right): average wind speeds in different dispersing processes per city. The circles represent the value of the parameters in each city. The percentiles of the box and whisker plots are consistent with those shown in Fig. 6. (For interpretation of the references to colour in this figure legend, the reader is referred to the web version of this article.)

quickly when there was a higher wind speed. The precipitation ratios, i.e., the ratio of the number of events with precipitation to 48 events in different dispersing processes was also calculated as the indicator of wet removal. Notably, the precipitation ratios of the 58 cities in the Rapid-Removal process were between 50% and 60%, which were much greater than those in the Slow-Removal process (average ratio of 35%) (Fig. 13). This result indicated that wet removal may be more effective for a thorough pollution cleaning for the whole NC region.

5. Conclusion

The air pollution in NC is severe, with domain-averaged $PM_{2.5}$ concentrations equal to 110, 68, 56 and 69 μg m^{-3} in winter, spring, summer and autumn, respectively, during 2013–2017. Based on in situ environmental and meteorological data over 16–58 cities, as well as the ERA-Interim reanalysis dataset, we explored the regional pollution characteristics and meteorological formation mechanism of $PM_{2.5}$ in NC during 2013–2017. Our main findings and conclusions are summarized below.

We developed two automatic algorithms to identify DRPTs and PRPEs in NC. Generally, the domain-averaged concentrations for Clear, Local-P, Small-C-P, Small-B-P, Large-P, and Large-S-P types were 39 ± 8, 53 ± 6, 60 ± 8, 73 ± 10, 94 ± 18 and 161 ± 39 μg m^{-3}, respectively, during 2014–2017. Clear days increased significantly from year to year in all four seasons, with the largest growth observed in summer. In contrast, Large-Region-P days had downward trends with the smallest decreases in winter. The average concentration of PRPEs also declined from 92 μg m^{-3} (2014) to 74 μg m^{-3} (2017); meantime, the number and duration of the PRPEs decreased. More than half of the air pollution events occurred in winter, with an average duration of 10.8 days. Compared with the typical event duration (3–5 days) in Beijing (Zheng et al. 2016), regional air pollution events over NC last longer. The evolution of the PRPEs in NC indicated that the area south of Hebei was the key area for the development of the PRPEs.

Twenty-six weather types (11 combined circulations) over NC were identified using the Lamb-Jenkinson weather typing classification method. Highly polluted types were mainly related to the C, southern (types S, SE, and SW) and eastern (type E) circulations, whereas less polluted types were the A, northern (type N) and western circulations (type W). In general, the contributions of interannual variability to $PM_{2.5}$ influenced by variations in circulation ranged from 40% to 65% in 16 cities, and meteorological contributions to the interannual domain-averaged $PM_{2.5}$ reduction in 2013 and 2017 were 64%, 58% and 45% in summer, autumn and winter, respectively. Based on the evolution of the PRPEs, type A circulation days decreased, while southern (types S and SW) and eastern (types E and SE) circulation days increased, from the starting stage to the peak stage. The number of anticyclone-related and northern (type N) circulation days increased from the peak stage to the ending stage. In addition, the RH and Rec increased first and then decreased gradually during the evolution of the PRPEs, while WS and BLH exhibited the opposite trend. A thorough and quick pollution cleaning for the whole NC region is closely related to a wide extent of wet removal (more than 50% cities had precipitation) and higher WSs (faster than 2.6 m s^{-1}). Furthermore, to explore atmospheric circulation and dynamic mechanisms, three typical circulation patterns were categorized in the peak stage of the PRPEs, namely, the southerly airflow pattern, the northerly airflow pattern and anticyclone pattern, and the NC region was completely controlled by a sinking motion in the mid-lower troposphere during these three circulation patterns.

Although the $PM_{2.5}$ concentration had a significant decline in 2017 compared to those in 2013, the $PM_{2.5}$ concentration in NC is still high and far exceeds the annual NAAQS II (35 μg m^{-3}) and the annual WHO Air Quality Guideline concentration (15 μg m^{-3}). It would take a long time to improve this condition. In addition, the meteorological contribution accounted for a large proportion of this reduction. Therefore, the implementation of emission reduction measures should be enhanced under unfavorable meteorological conditions, especially in the southern part of Hebei Province to reduce the intensity and frequency of regional pollution events.

Author contribution

LL Wang put forward the idea of this research. MG Li and LL Wang mainly participated in data processing and analysis and wrote the paper. Weather type classification and PM2.5 reconstruction program is provided by JD Liu. Y Sun, WK Gao, L Li and T Song provided partially PM 2.5 data. L Liu provided partially meteorological data. All the authors commented and participated in the revision of the paper.

Declaration of Competing Interest

The authors declare that they have no conflict of interest.

Acknowledgements

This work was partially supported by the grant of National Key R&D Plan (Quantitative Relationship and Regulation Principle between Regional Oxidation Capacity of Atmospheric and Air Quality 2017YFC0210003), the National Natural Science Foundation of China (No. 41505133 & 41775162), the Strategic Priority Research Program of the Chinese Academy of Sciences (No. XDA19020303), Beijing Major Science and Technology Project 510 (Z181100005418014), National

research program for key issues in air pollution control (DQGG0101) and the China Scholarship Council fellowship (201804910025 & 201904910518). Special thanks to the National Earth System Science, Data Sharing Infrastructure, and National Science & Technology Infrastructure of China. We thank European Research Council via ATM-GTP 266 (742206), and Academy of Finland Centre of Excellence in Atmospheric Sciences (272041).

Appendix A. Supplementary material

Supplementary data to this article can be found online at https://doi.org/10.1016/j.envint.2019.105283.

References

Allwine, K.J., Whiteman, C.D., 1994. Single-station integral measures of atmospheric stagnation recirculation and ventilation. Atmos Environ. 28, 713–721.
Andreadis, K.M., Clark, E.A., Wood, A.W., Hamlet, A.F., Lettenmaier, D.P., 2005. Twentieth-century drought in the conterminous United States. J. Hydrometeorol. 6, 985–1001.
Burnett, R.T., Pope, C.A., Ezzati, M., Olives, C., Lim, S.S., Mehta, S., Shin, H.H., Singh, G., Hubbell, B., Brauer, M., Anderson, H.R., Smith, K.R., Balmes, J.R., Bruce, N.G., Kan, H.D., Laden, F., Pruss-Ustun, A., Michelle, C.T., Gapstur, S.M., Diver, W.R., Cohen, A., 2014. An integrated risk function for estimating the global burden of disease attributable to ambient fine particulate matter exposure. Environ. Health Persp. 122, 397–403.
Cai, W., Li, K., Liao, H., Wang, H., Wu, L., 2017. Weather conditions conducive to Beijing severe haze more frequent under climate change. Nat. Clim. Change 7, 257–262.
Chen, Z., Xie, X., Cai, J., Chen, D., Gao, B., He, B., Cheng, N., Xu, B., 2018. Understanding meteorological influences on $PM_{2.5}$ concentrations across China: a temporal and spatial perspective. Atmos. Chem. Phys. 18, 5343–5358.
Chen, Z.H., Cheng, S.Y., Li, J.B., Guo, X.R., Wang, W.H., Chen, D.S., 2008. Relationship between atmospheric pollution processes and synoptic pressure patterns in northern China. Atmos. Environ. 42, 6078–6087.
Cheng, Z., Luo, L., Wang, S., Wang, Y., Sharma, S., Shimadera, H., Wang, X., Bressi, M., de Miranda, R.M., Jiang, J., Zhou, W., Fajardo, O., Yan, N., Hao, J., 2016. Status and characteristics of ambient $PM_{2.5}$ pollution in global megacities. Environ. Int. 89–90, 212–221.
Comrie, A.C., Yarnal, B., 1992. Relationships between synoptic-scale atmospheric circulation and ozone concentrations in metropolitan pittsburgh Pennsylvania. Atmos. Environ. B-Urb 26, 301–312.
Hegarty, J., Mao, H., Talbot, R., 2007. Synoptic controls on summertime surface ozone in the northeastern United States. J. Geophys. Res. 112.
Huang, R.J., Zhang, Y.L., Bozzetti, C., Ho, K.F., Cao, J.J., Han, Y.M., Daellenbach, K.R., Slowik, J.G., Platt, S.M., Canonaco, F., Zotter, P., Wolf, R., Pieber, S.M., Bruns, E.A., Crippa, M., Ciarelli, G., Piazzalunga, A., Schwikowski, M., Abbaszade, G., Schnelle-Kreis, J., Zimmermann, R., An, Z.S., Szidat, S., Baltensperger, U., El Haddad, I., Prevot, A.S.H., 2014. High secondary aerosol contribution to particulate pollution during haze events in China. Nature 514, 218–222.
Jones, P.D., Hulme, M., Briffa, K.R., 1993. A Comparison of lamb circulation types with an objective classification scheme. Int. J. Climatol. 13, 655–663.
Lamb, H.H. British, 1972. Isles weather types and a register of the daily sequence of circulation patterns 1861–1971. London H.M. Stationery Off.
Leung, D.M., Tai, A.P.K., Mickley, L.J., Moch, J.M., van Donkelaar, A., Shen, L., Martin, R.V., 2018. Synoptic meteorological modes of variability for fine particulate matter ($PM_{2.5}$) air quality in major metropolitan regions of China. Atmos. Chem. Phys. 18, 6733–6748.
Li, T., Guo, Y., Liu, Y., Wang, J., Wang, Q., Sun, Z., He, M.Z., Shi, X., 2019b. Estimating mortality burden attributable to short-term $PM_{2.5}$ exposure: a national observational study in China. Environ. Int. 125, 245–251.
Li, Z.Q., Lau, W.K.M., Ramanathan, V., Wu, G., Ding, Y., Manoj, M.G., Liu, J., Qian, Y., Li, J., Zhou, T., Fan, J., Rosenfeld, D., Ming, Y., Wang, Y., Huang, J., Wang, B., Xu, X., Lee, S.S., Cribb, M., Zhang, F., Yang, X., Zhao, C., Takemura, T., Wang, K., Xia, X., Yin, Y., Zhang, H., Guo, J., Zhai, P.M., Sugimoto, N., Babu, S.S., Brasseur, G.P., 2016b. Aerosol and monsoon climate interactions over Asia. Rev. Geophys. 54, 866–929.
Li, J., Li, C.C., Zhao, C.S., Su, T.N., 2016a. Changes in surface aerosol extinction trends over China during 1980–2013 inferred from quality-controlled visibility data. Geophys. Res. Lett. 43, 8713–8719.
Li, J., Liao, H., Hu, J., Li, N., 2019a. Severe particulate pollution days in China during 2013–2018 and the associated typical weather patterns in Beijing-Tianjin-Hebei and the Yangtze River Delta regions. Environ. Pollut. 248, 74–81.
Liao, H., Chang, W.Y., Yang, Y., 2015. Climatic Effects of Air Pollutants over China: A Review. Adv. Atmos. Sci. 32, 115–139.
Liao, T., Gui, K., Jiang, W., Wang, S., Wang, B., Zeng, Z., Che, H., Wang, Y., Sun, Y., 2018. Air stagnation and its impact on air quality during winter in Sichuan and Chongqing, southwestern China. Sci. Total Environ. 635, 576–585.
Ma, Q., Wu, Y., Zhang, D., Wang, X., Xia, Y., Liu, X., Tian, P., Han, Z., Xia, X., Wang, Y., Zhang, R., 2017. Roles of regional transport and heterogeneous reactions in the $PM_{2.5}$ increase during winter haze episodes in Beijing. Sci. Total Environ. 599–600, 246–253.
Maji, K.J., Ye, W.F., Arora, M., 2018. Shiva Nagendra, S.M. $PM_{2.5}$-related health and economic loss assessment for 338 Chinese cities. Environ. Int. 121, 392–403.
Ren, F.M., Cui, D.L., Gong, Z.Q., Wang, Y.J., Zou, X.K., Li, Y.P., Wang, S.G., Wang, X.L., 2012. An objective identification technique for regional extreme events. J. Climate 25, 7015–7027.
Song, C., Wu, L., Xie, Y., He, J., Chen, X., Wang, T., Lin, Y., Jin, T., Wang, A., Liu, Y., Dai, Q., Liu, B., Wang, Y.N., Mao, H., 2017. Air pollution in China: status and spatio-temporal variations. Environ. Pollut. 227, 334–347.
Sun, Y., Du, W., Wang, Q., Zhang, Q., Chen, C., Chen, Y., Chen, Z., Fu, P., Wang, Z., Gao, Z., Worsnop, D.R., 2015. Real-time characterization of aerosol particle composition above the urban canopy in beijing: insights into the interactions between the atmospheric boundary layer and aerosol chemistry. Environ. Sci. Technol. 49, 11340–11347.
Sun, Y.L., Wang, Z.F., Fu, P.Q., Jiang, Q., Yang, T., Li, J., Ge, X.L., 2013. The impact of relative humidity on aerosol composition and evolution processes during wintertime in Beijing. China. Atmos Environ 77, 927–934.
Tang, G., Zhang, J., Zhu, X., Song, T., Münkel, C., Hu, B., Schäfer, K., Liu, Z., Zhang, J., Wang, L., Xin, J., Suppan, P., Wang, Y., 2016. Mixing layer height and its implications for air pollution over Beijing China. Atmos. Chem. Phys. 16, 2459–2475.
Tao, M., Chen, L., Li, R., Wang, L., Wang, J., Wang, Z., Tang, G., Tao, J., 2016. Spatial oscillation of the particle pollution in eastern China during winter: implications for regional air quality and climate. Atmos. Environ. 144, 100–110.
Tao, M., Chen, L., Su, L., Tao, J., 2012. Satellite observation of regional haze pollution over the North China Plain. J. Geophys. Res.: Atmos. 117.
Trigo, R.M., DaCamara, C.C., 2000. Circulation weather types and their influence on the precipitation regime in Portugal. Int. J. Climatol. 20, 1559–1581.
Wang, H.-J., Chen, H.-P., 2016. Understanding the recent trend of haze pollution in eastern China: roles of climate change. Atmos. Chem. Phys. 16, 4205–4211.
Wang, H., Xu, J., Zhang, M., Yang, Y., Shen, X., Wang, Y., Chen, D., Guo, J., 2014a. A study of the meteorological causes of a prolonged and severe haze episode in January 2013 over central-eastern China. Atmos. Environ. 98, 146–157.
Wang, H., Zhao, L., 2018. A joint prevention and control mechanism for air pollution in the Beijing-Tianjin-Hebei region in china based on long-term and massive data mining of pollutant concentration. Atmos. Environ. 174, 25–42.
Wang, L., Wang, Y., Wang, Y., Sun, Y., Ji, D., Ren, Y., 2010. Relationship between different synoptic weather patterns and concentrations of atmospheric pollutants in Beijing during summer and autumn. China Environ. Sci. 30, 924–930.
Wang, L., Zhang, N., Liu, Z., Sun, Y., Ji, D., Wang, Y., 2014b. The influence of climate factors, meteorological conditions, and boundary-layer structure on severe haze pollution in the beijing-tianjin-hebei region during January 2013. Adv. Meteorol. 2014, 1–14.
Wang, X., Dickinson, R.E., Su, L., Zhou, C., 2017. Wang K. $PM_{2.5}$ pollution in china and how it has been exacerbated by terrain and meteorological conditions. Bull. Am. Meteorol. Soc.
Wang, Y., Ying, Q., Hu, J., Zhang, H., 2014c. Spatial and temporal variations of six criteria air pollutants in 31 provincial capital cities in China during 2013–2014. Environ. Int. 73, 413–422.
Wang, Y.S., Yao, L., Wang, L.L., Liu, Z.R., Ji, D.S., Tang, G.Q., Zhang, J.K., Sun, Y., Hu, B., Xin, J.Y., 2014d. Mechanism for the formation of the January 2013 heavy haze pollution episode over central and eastern China. Sci. China Earth Sci. 57, 14–25.
Wu, P., Ding, Y., Liu, Y., 2017. Atmospheric circulation and dynamic mechanism for persistent haze events in the Beijing–Tianjin–Hebei region. Adv. Atmos. Sci. 34, 429–440.
Ye, X., Song, Y., Cai, X., Zhang, H., 2016. Study on the synoptic flow patterns and boundary layer process of the severe haze events over the North China Plain in January 2013. Atmos. Environ. 124, 129–145.
Zhang, H., Yuan, H., Liu, X., Yu, J., Jiao, Y., 2018a. Impact of synoptic weather patterns on 24h-average $PM_{2.5}$ concentrations in the North China Plain during 2013–2017. Sci. Total Environ. 627, 200–210.
Zhang, Q., He, K.B., Huo, H., 2012. Cleaning China's air. Nature 484, 161–162.
Zhang, R.Y., Wang, G.H., Guo, S., Zarnora, M.L., Ying, Q., Lin, Y., Wang, W.G., Hu, M., Wang, Y., 2015. Formation of Urban fine particulate matter. Chem. Rev. 115, 3803–3855.
Zhang, Y., Ding, A.J., Mao, H.T., Nie, W., Zhou, D.R., Liu, L.X., Huang, X., Fu, C.B., 2016. Impact of synoptic weather patterns and inter-decadal climate variability on air quality in the North China Plain during 1980–2013. Atmos. Environ. 124, 119–128.
Zhang, H., Yuan, H.O., Liu, X.H., Yu, J.Y., Jiao, Y.L., 2018b. Impact of synoptic weather patterns on 24 h-average $PM_{2.5}$ concentrations in the North China Plain during 2013–2017. Sci. Total Environ. 627, 200–210.
Zhao, B., Wu, W., Wang, S., Xing, J., Chang, X., Liou, K.-N., Jiang, J.H., Gu, Y., Jang, C., Fu, J.S., Zhu, Y., Wang, J., Lin, Y., Hao, J., 2017. A modeling study of the nonlinear response of fine particles to air pollutant emissions in the Beijing–Tianjin–Hebei region. Atmos. Chem. Phys. 17, 12031–12050.
Zhao, S., Yu, Y., Yin, D., He, J., Liu, N., Qu, J., Xiao, J., 2016. Annual and diurnal variations of gaseous and particulate pollutants in 31 provincial capital cities based on in situ air quality monitoring data from China national environmental monitoring center. Environ. Int. 86, 92–106.
Zheng, G., Duan, F., Ma, Y., Zhang, Q., Huang, T., Kimoto, T., Cheng, Y., Su, H., He, K., 2016. Episode-based evolution pattern analysis of haze pollution: method development and results from Beijing China. Environ. Sci. Technol. 50, 4632–4641.
Zheng, G.J., Duan, F.K., Su, H., Ma, Y.L., Cheng, Y., Zheng, B., Zhang, Q., Huang, T., Kimoto, T., Chang, D., Pöschl, U., Cheng, Y.F., He, K.B., 2015. Exploring the severe winter haze in Beijing: the impact of synoptic weather, regional transport and heterogeneous reactions. Atmos. Chem. Phys. 15, 2969–2983.
Zhu, X., Tang, G., Guo, J., Hu, B., Song, T., Wang, L., Xin, J., Gao, W., Münkel, C., Schäfer, K., Li, X., Wang, Y., 2018. Mixing layer height on the North China Plain and meteorological evidence of serious air pollution in southern Hebei. Atmos. Chem. Phys. 18, 4897–4910.
Zhu, X.W., Tang, G.Q., Hu, B., Wang, L.L., Xin, J.Y., Zhang, J.K., Liu, Z.R., Munkel, C., Wang, Y.S., 2016. Regional pollution and its formation mechanism over North China Plain: a case study with ceilometer observations and model simulations. J. Geophys. Res.-Atmos. 121, 14574–14588.